IOSR Journal of Applied Chemistry (IOSR-JAC)
e-ISSN: 2278-5736.Volume 19, Issue 6 Ser. I (June. 2026), PP 42-53
www.iosrjournals.org

Permanganate-mediated oxidation of *Pachira aquatica* shells as biosorbent for Chromium detoxification in Water

Owolabi Mutolib Bankole
Hydrochemistry Research Laboratory, Department of Chemical Sciences, Adekunle Ajasin University, Akungba Akoko, Nigeria

Abstract
In this study, shells of money tree chestnuts (Pachira aquatic, MT) were oxidatively modified using potassium permanganate to produce a MnOx-functionalized biosorbent (mMT) for efficient removal of hexavalent chromium (Cr(VI)) from aqueous media. Surface oxidation with $KMnO_4$ significantly enhanced the adsorption performance by introducing oxygen-containing functional groups and Mn-based redox sites on the biomass surface. Adsorption experiments showed that Cr(VI) uptake increased with increasing concentration and was best described by the Langmuir model, yielding a maximum adsorption capacity of 179.31 mg/g. Sorption kinetics reached equilibrium within 60 min and were best fitted by the pseudo-second-order model, suggesting that chemisorption governs the rate-limiting step. The surface chemistry and structural changes of the materials were investigated using FTIR, SEM-EDX), XRD, and TGA analyses. The modified biomass exhibited strong pH-dependent behavior, achieving nearly complete Cr(VI) removal at pH 2.5 due to the combined effects of electrostatic attraction and surface-mediated redox interactions. Interference studies revealed moderate effects of coexisting ions, with phosphate showing the strongest competition for adsorption sites. Regeneration experiments using NaOH demonstrated that the sorbent retained approximately 75% of its initial adsorption capacity after five cycles.

Keywords: *Money tree chestnut shell; $KMnO_4$ modification; hexavalent chromium; biomass functionalization; wastewater treatment; surface redox-active sites.*

Date of Submission: 09-06-2026 Date of Acceptance: 19-06-2026

I. Introduction

Hexavalent chromium, (Cr(VI)), is among the most hazardous inorganic contaminants commonly detected in industrial wastewater [1,2]. Its high solubility and mobility in aqueous environments enable it to migrate readily through soil and water systems [2], thereby posing persistent risks to ecosystems and human health. In water, Cr(VI) predominantly exists as chromate (CrO_4^{2-}), hydrogen chromate ($HCrO_4^-$), and dichromate ($Cr_2O_7^{2-}$) species that can easily penetrate biological membranes due to their small size and strong oxidizing nature [3]. Once internalized, Cr(VI) may induce oxidative stress, DNA damage, and carcinogenic effects [2], making its removal from contaminated water a critical environmental priority. Consequently, considerable research attention has shifted toward the development of biomass-derived sorbents capable of removing toxic Cr(VI) species from aqueous media.

Lignocellulosic biomass has emerged as an attractive precursor for low-cost adsorbents because of its natural abundance, renewability, and intrinsic surface chemistry [4,5]. Agricultural residues are composed mainly of cellulose, hemicellulose, and lignin, which collectively provide a framework rich in hydroxyl, phenolic, and ether functionalities capable of interacting with metal ions [5]. These functional groups can participate in adsorption processes through electrostatic attraction, hydrogen bonding, surface complexation, and in some cases redox interactions [6]. However, untreated biomass materials frequently exhibit modest adsorption performance due to limited accessibility of active sites, surface passivation, and relatively low surface polarity [6]. As a result, chemical modification strategies are commonly employed to enhance the adsorption capacity of biomass by introducing additional functional groups and improving the structural accessibility of binding sites [7].

A variety of oxidizing agents have been investigated to activate biomass-derived adsorbents by introducing additional surface functionalities and improving structural accessibility. For instance, H_2O_2 has been used as a mild oxidant to generate oxygen-containing functional groups on carbon surfaces; Murtazaoğlu and co-workers reported that H_2O_2-treated activated carbon exhibited increased densities of surface oxygen functionalities and enhanced adsorption of Cu^{2+} and Zn^{2+} ions due to improved hydrophilicity and pore accessibility [8]. Acid-based oxidative treatments have also proven effective in tailoring biomass surfaces. Li Zhang and colleagues modified bagasse using H_3PO_4, HNO_3, and $C_2H_2O_4$, producing adsorbents with increased surface area, larger pore volume, and higher concentrations of oxygen-containing functional groups, which significantly improved Cr(VI) removal [9]. Similarly, H_3PO_4-activated cocopeat biochar reported by Sireesha and

Sreedhar exhibited enhanced porosity and phosphorus-containing surface groups that facilitated efficient adsorption of Cu^{2+} and Ni^{2+} ions from aqueous and real wastewater systems [11]. Incorporation of oxidized biochar into polymeric matrices has further improved adsorption performance; for instance, a H_3PO_4-modified biochar-chitosan nanocomposite containing abundant -NH_2, -OH, and -COOH groups demonstrated effective removal of several heavy metals including Cu^{2+}, Ni^{2+}, and, Zn^{2+} [11]. Other oxidants such as HNO_3 and ammonium persulfate (APS) have also been employed to introduce reactive oxygenated groups and enhance surface reactivity. HNO_3-modified biomass has shown significantly improved Pb^{2+} adsorption through additional -COO^- and -OH^- binding sites [12], while APS-modified chitosan-derived biochar and activated carbon fibers have demonstrated increased surface area for removal of Cr(VI) [13], tetracycline antibiotics [13], and $Pb^{2+}$from contaminated water [14].

Potassium permanganate ($KMnO_4$) has attracted significant interest due to its strong oxidative potential and multifunctional role in surface modification. $KMnO_4$ has standard reduction potential of about +1.51 V in acidic media which can oxidize alcohol, aldehyde, and phenolic groups in lignocellulosic materials [15], while Mn(VII) is simultaneously reduced to lower-valence manganese oxides such as MnO_2 or Mn_2O_3 and deposit on the biomass surface [16]. This dual process produces a hybrid material with both adsorption and redox properties. Previous studies have shown that $KMnO_4$-modified biomass, including corncob [17], hydrochar [18], and bamboo biochar [19], exhibits enhanced removal of heavy metals and dyes due to the combined effects of MnO_x particles and newly introduced functional groups that promote electrostatic attraction, surface complexation, and redox interactions. In addition, $KMnO_4$ modification generates surface acidic groups more effectively than conventional mineral acids and does not produce large volume of acidic wastes [20]. It also possesses superior oxidation capacity compared to APS and H_2O_2 due to its multi-electron transfer capabilities [21,22].

Herein, the present study explores the use of empty shells of money tree chestnuts (*Pachira aquatica*) as a sustainable precursor for the development of a $KMnO_4$-modified biosorbent for Cr(VI) removal from aqueous solution. Chestnut shells represent an abundant agricultural by-product that is typically discarded despite possessing a lignocellulosic framework rich in reactive functional groups. Through $KMnO_4$ oxidation, the surface chemistry of this biomass can be significantly enhanced while simultaneously introducing MnOx species capable of participating in redox reactions. Such modification is expected to generate a multifunctional adsorbent in which oxygenated surface groups promote electrostatic binding of Cr(VI) oxyanions, while surface-associated Mn(III)/Mn(IV) species facilitate the reduction of Cr(VI) to the less toxic Cr(III) form. By transforming an otherwise underutilized biomass residue into a value-added material, this approach provides a sustainable pathway for waste valorization and water purification. The structural and chemical characteristics of the modified biosorbent were therefore systematically investigated, and its performance toward Cr(VI) removal was evaluated through kinetic, equilibrium, and thermodynamic studies in order to elucidate the underlying adsorption and reduction mechanisms.

II. Materials and methods

2.1 Materials

The reagents used in this work, including $K_2Cr_2O_7$, $KMnO_4$, Abs ethanol (99%), and NaOH pellets, were purchased from Sigma Aldrich and were used as received without further purification. Deionized water, NaCl, and HCl (37%) were supplied by Pascal Chemical Limited, Nigeria. Pristine empty shell of money tree chestnuts (MT) were generously supplied by the Department of Plant Science and Biotechnology at Adekunle Ajasin University, Nigeria. A stock solution of Cr(VI) (1000 mg/L) was prepared by dissolving 2.83 g of $K_2Cr_2O_7$ in deionized water and making up the volume to 1 L, based on its 35.35% Cr(VI) content.

2.2 Methods

2.2.1 MT shell Modification with $KMnO_4$

The biomass (*Pachira aquatica*) was initially rinsed with tap water to remove surface debris, then soaked in 1% HCl to eliminate residual impurities, followed by repeated washing with deionized water until a neutral pH was achieved. It was subsequently dried at 80 ± 3 °C to constant weight, ground, and sieved through a 0.25 mm mesh to obtain the unmodified sample (MT).

For modification, 10 g of the powdered biomass was dispersed in 100 mL of 0.05 M $KMnO_4$, sonicated for 30 min, and then refluxed for 1 h in 250 mL conical flasks. After cooling and standing for 2 h to complete oxidation, the biomass was filtered using a Buchner funnel, rinsed with deionized water until clear, and oven-dried at 100 °C for 24 h to yield the modified biomass (mMT).

2.2.2 Batch Adsorption Studies

The impact of oxidative modification on Cr(VI) adsorption was examined through batch experiments. A fixed dose of 50 mg mMT was dispersed in 100 mL of 100 mg/L Cr(VI) solution and stirred at 150 rpm until

equilibrium. At predetermined intervals, aliquots were withdrawn, filtered, and the residual Cr(VI) concentration in the filtrate was determined using a standard calibration curve (y = 0.0676x + 0.0346; R^2 = 0.999] constructed from Cr(VI) solutions (1-5 mg/L) at the λ_{max} of Cr(VI) on a UV/vis spectrophotometer, Figure 1. Kinetic studies were conducted at room temperature over a 1-60 min range using 50 mg of mMT at pH 2.5.0 ± 0.1 with 100 mg/L Cr(VI) solution. For isotherm studies, initial Cr(VI) concentrations ranging from 10 to 100 mg/L were stirred for 60 min under similar conditions, and residual concentrations were determined as described above. Removal efficiency (%) and adsorption capacity (q_e) were calculated using **Eqns. 1** and **2**, respectively.

.Removal rate (%) $= \frac{c_o - c_t}{c_o} \times 100$ **1**

$q_e = (c_o - c_e)V/m$ **2**

In the formula, c_o (mg/L) is the initial concentration of Cr(VI), c_t (mg/L) is the concentration of Cr(VI) after time t of contact with adsorbents, c_e (mg/L) is the residual pollutant concentrations at equilibrium, V (mL) is the volume of the pollutants, m (mg) is the mass of the adsorbent added, and q_e (mg/g) is the adsorption capacity at equilibrium.

The adsorption process was also investigated under varying solution pH and in the presence of different interfering anions to determine the effects of these factors on the adsorption performance of mMT. For the effects of solution pH, 30 mg of adsorbent was separately dispersed into 20 mL of Cr(VI) (50 mg/L) solutions in 40 mL vials, and the pH of each solution was adjusted within the range of 2.0 - 10. To examine the potential interference of anions like Mg^{2+}, NO_3^-, Na^+, Ca^{2+}, CO_3^{2-}, PO_4^{3-}, SO_4^{2-}, on the adsorption performance was tested in aqueous solutions of $MgCl_2$, NaCl, $NaNO_3$, $CaCl_2$, Na_2CO_3, Na_3PO_4, Na_2SO_4, respectively.

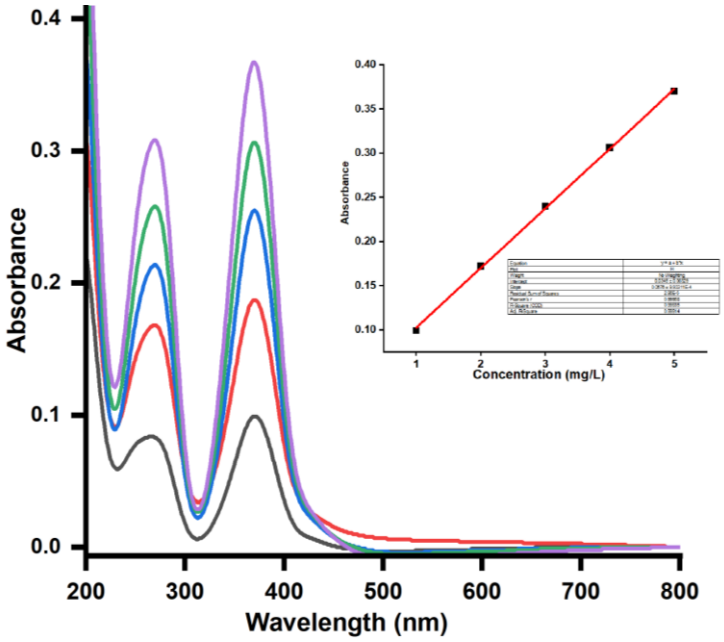

Figure 1:

2.3 Materials Characterization

X-ray Diffraction: The XRD spectra were obtained with Bruker D8 ADVANCE diffractometer (Germany) using Cu Kα (1.5406 Å) radiation, a voltage of 40 kV, and a generator current of 35 mA. The scanning scope angle (2θ) varied from 10–80 degrees at room temperature.

Scanning electron microscope (SEM)/energy dispersive X-ray: The surface morphology and elemental composition of the sorbents were analyzed using SEM equipped with energy dispersive analysis of X-ray equipment (EDAX) (XL 30 FEG ESEM).

Fourier Transmitted Infra-Red Spectroscopy (FTIR): The surface functional groups on the samples were recorded on a Thermo Fisher Scientific FTIR spectrophotometer, using pressed KBr pellets.

2.5 Determination of pH of point zero charge (pH PZC)

The pH of point zero charge (PZC) was determined using the solid addition method viz [23]: to a series of 100 mL conical flasks, 40 mL of 0.1M KNO_3 solution was transferred. The initial pH (pH 0) values of the solution were adjusted from 2 to 10 by adding either 0.1N H_2SO_4 or NaOH. The total volume of the solution in each flask was made exactly to 50ml by adding the KNO_3 solution. Then 0.05g of sample was added to each flask and securely capped immediately. The suspension was then manually agitated for 24h. The pH values of the

supernatant liquid were noted after 24 h and denoted as pH_f. The difference between the initial (pH_0) and final pH (pH_f) values ($\Delta pH = pH_0 - pH_f$) was plotted against the pH_0. The point of intersection of the resulting curve at which ΔpH equals zero gave the PZC.

III. Results and discussion

The surface functionalities of both pristine and permanganate-modified biomass were elucidated using FTIR spectroscopy, and their respective spectra are displayed in Figure 1a. In the unmodified biomass, a broad vibrational band centered at 3324 cm^{-1} corresponds to OH stretching due to adsorbed moisture. A small but visible band at ~2905 cm^{-1} is attributed to the C–H stretching vibration in the biomass backbone, Figure 1a. Other vibrational bands at 1607.02, 1531.23, and 1038.3 cm^{-1} correspond to the -COO-, C-C, and C-O bonds, respectively. In the spectrum of the modified biomass (mMT), the OH and C-H vibrational stretchings appear broader and more intense compared to the unmodified spectrum (MT), indicating the successful oxidation of the biomass with permanganate. Notably, the presence of carbonyl groups on the surface of the oxidized biomass is indicated by the peak at ~1724.4 cm^{-1} [24]. Moreover, vibrational bands at 1029, 1255, and 1624 cm^{-1}, corresponding to C-O, OH bending, and -COO- groups, respectively, exhibit greater intensity in the modified biomass compared to the unmodified biomass spectrum.

Both modified and unmodified biomass responses to temperature were analyzed via thermogravimetry analysis in the 30-800 °C range, with a heating rate of 25.00 °C/min under N_2, Figure 2b. The TGA curve for MT exhibited two degradation stages: the first at 180 °C, resulting in a 4.6% mass loss attributed to adsorbed water removal, and the second step at 201-800 °C, with a 32% mass loss due to direct biomass decomposition. The mMT profile displayed three stages at 171 °C (9.12% mass loss), 180-365 °C (42.2% mass), and 368-800 °C (64.6% mass loss), corresponding to moisture evaporation, MnO_2 phase transition to Mn_3O_4 [25]. and organic residue pyrolysis. The process of oxidation accelerated the decomposition rate of mMT [26], leading to a more significant mass loss compared to unmodified biomass.

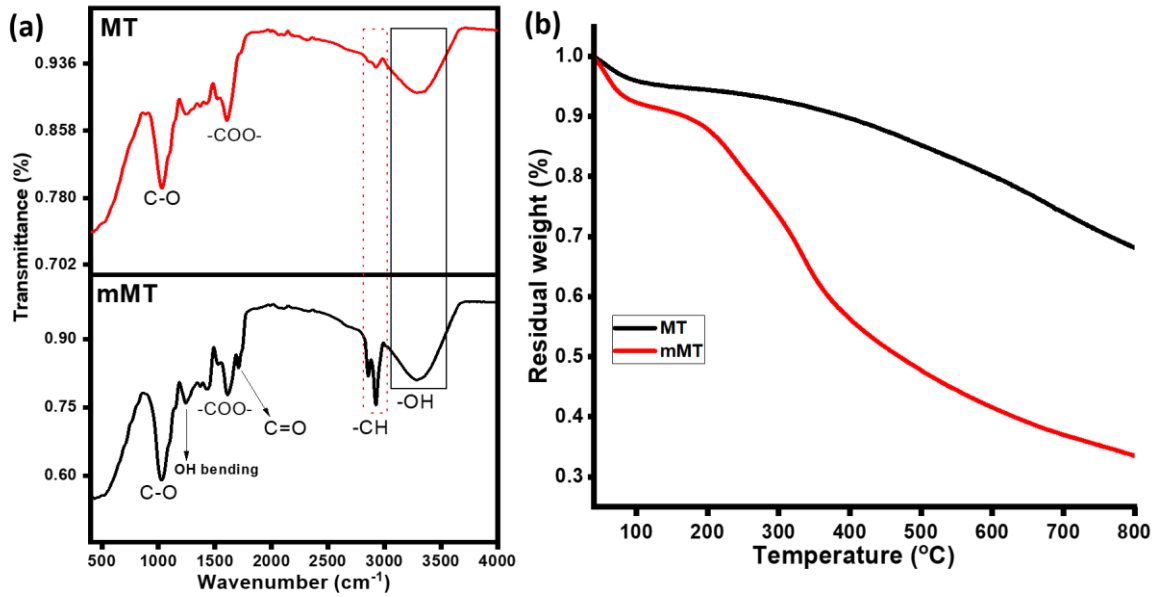

Figure 2: FTIR spectra and TGA profiles of modified and unmodified biomass.

The SEM analysis reveals clear morphological differences between unmodified and $KMnO_4$-modified biomass, Figure 3. The unmodified biomass exhibits a rough, irregular surface with visible porosity, fragmented textures, and prominent ridges and cavities, indicative of its natural structure. In contrast, the $KMnO_4$-modified biomass shows a smoother, more compact morphology, suggesting that $KMnO_4$ treatment significantly alters the surface structure, reducing porosity and introducing fine fibril-like features.

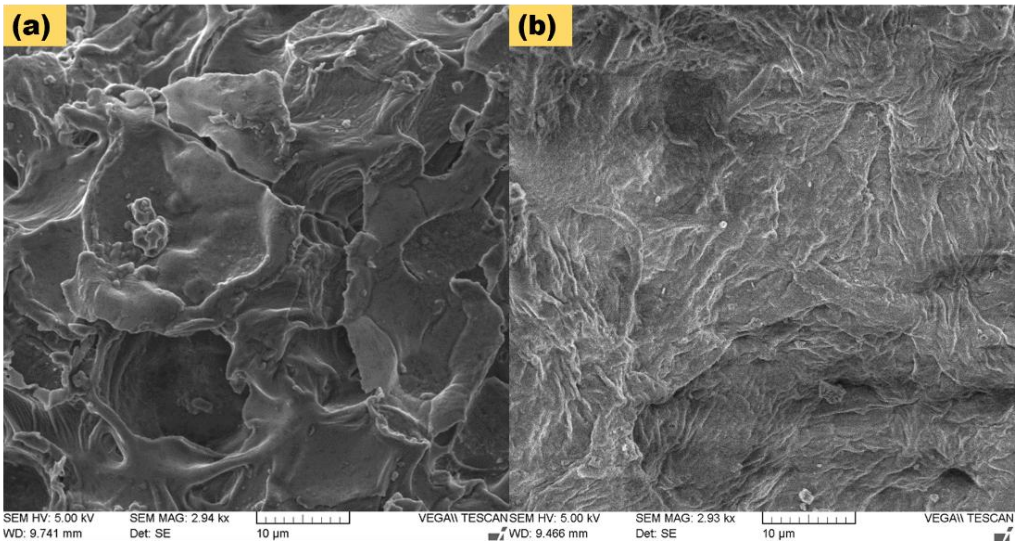

Figure 3: Scanning electron microscope (SEM) images of modified and unmodified biomass.

The energy-dispersive X-ray (EDX) spectra of unmodified biomass (a) and biomass modified with KMnO4 (b) display significant differences in their elemental compositions, Figure 4. The EDX spectrum of unmodified biomass is characterized by prominent peaks corresponding to C and O, which are typical for organic materials. Additionally, smaller peaks for potassium (K), calcium (Ca), magnesium (Mg), and chlorine (Cl) are observed, reflecting the natural mineral content of the biomass. In contrast, the EDX spectrum of the $KMnO_4$-modified biomass reveals the presence of new peaks for manganese (Mn), indicating successful incorporation of Mn from the $KMnO_4$ treatment.

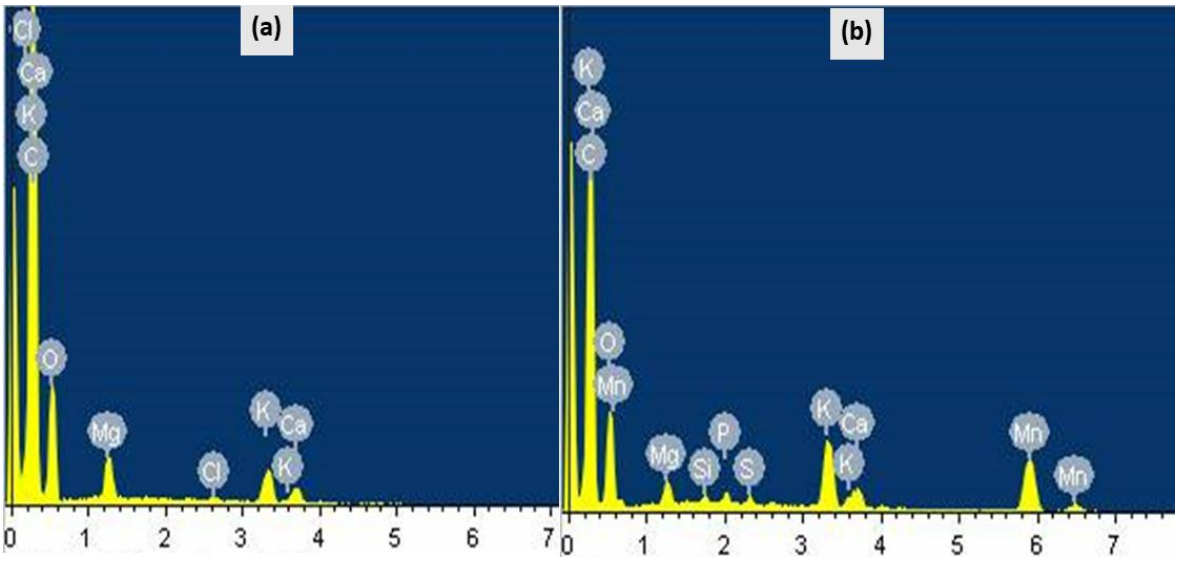

Figure 4: EDX spectra of unmodified biomass (a) and biomass modified with $KMnO_4$ (b)

The XRD patterns of pristine biomass (MT) and modified biomass (mMT) are shown in Figure 5. The pristine biomass exhibits a broad diffraction band centered around $2\theta = 20.34^o$, which is typical of amorphous lignocellulosic materials, including the disordered structure of cellulose, lignin, and hemicellulose [27]. The broad feature indicates that pristine biomass is non-crystalline. The XRD image of mMT shows a similar broad peak around $2\theta = 22.24^o$ and with reduced intensity, suggesting partial disruption or structural rearrangement of the original lignocellulosic materials due to surface oxidation by $KMnO_4$. The absence of sharp crystalline phases in both patterns confirms that the materials remain largely amorphous after modification.

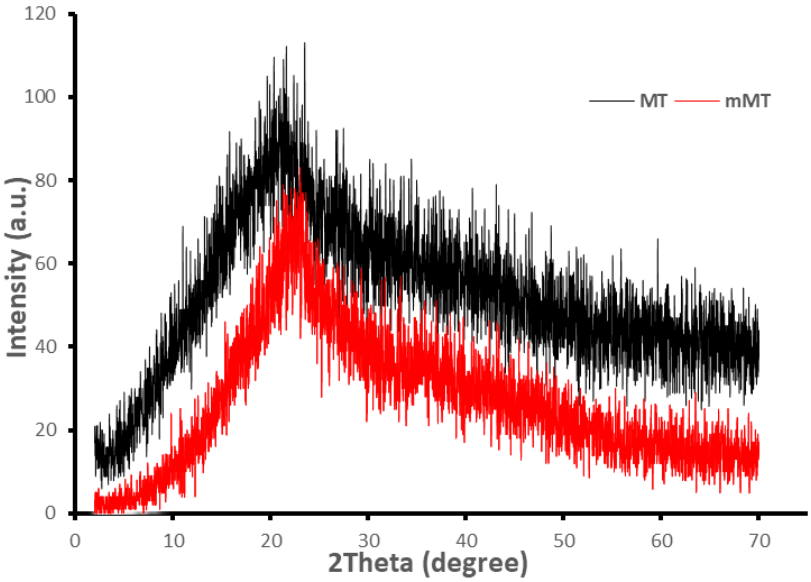

Figure 5: XRD patterns of unmodified biomass (black) and biomass modified with $KMnO_4$ (red)

Batch Adsorption Experiment

Effect of pH on Cr(VI) adsorption

The pH-dependent performance of mMT was evaluated over a range of 2.5 to 10.5 using a 100 mg/L Cr(VI) solution. As shown in Figure 6a, the Cr(VI) removal efficiency declined progressively with increasing pH, with removal values of ~99.99% at pH 2.5, 92.34% at pH 4.5, 62.39% at pH 6.5, 28.22% at pH 8.5, and 18.1% at pH 10.5. The pronounced removal at low pH is attributed to the combined effect of electrostatic attraction and surface-mediated redox activity [28-30]. Cr(VI) exists in aqueous solution as different oxyanions depending on pH. In solution, Cr(VI) exists as $HCrO_4^-$ and $Cr_2O_7^{2-}$, below pH 6, and as CrO_4^{2-} at higher pH [31], following **Eqns. 3-6**:

$$K_2Cr_2O_7 + H_2O \rightarrow 2K^+ + Cr_2O_7^{2-} + OH^- + H^+ \quad (3)$$

$$Cr_2O_7^{2-} + H_2O \rightarrow 2HCrO_4^-, pKa = 2.2 \quad (4)$$

$$H_2CrO_4^{2-} \rightarrow HCrO_4^- + H^+, pKa = 4.1 \quad (5)$$

$$HCrO_4^- \rightarrow CrO_4^{2-} + H^+, pKa = 5.9 \quad (6)$$

Simultaneously, the mMT surface undergoes pH-dependent speciation [32], with surface protonation prevailing under acidic conditions and deprotonation under basic conditions, as represented in **Eqns. 7** and **8**, respectively.

$$mMT - OH_2^+ \rightarrow mMT - OH + H^+ \quad (pH < pH_{PZC}) \quad (7)$$

$$mMT - OH \rightarrow mMT - O^- + H^+ \quad (pH > pH_{PZC}) \quad (8)$$

Below the point of zero charge ($pH_{PZC} \approx 4.4$), mMT carries a net positive surface charge, favoring electrostatic attraction of Cr(VI) anions and favouring both adsorption and reduction. At higher pH (≥ 6.5), CrO_4^{2-} becomes the dominant species, and the mMT surface is deprotonated and negatively charged. These changes result in electrostatic repulsion and increased competition from OH^-, significantly diminishing Cr(VI) uptake. Therefore, acidic conditions (pH 2.5-4.5) provide the most favorable environment for Cr(VI) removal via both adsorption and redox conversion, while alkaline conditions hinder performance due to reduced surface activity and unfavorable Cr(VI) speciation. Acidic conditions were selected to elucidate intrinsic adsorption behaviour; practical implementation may involve pre-acidification or integration with acidic industrial streams. Based on these findings, subsequent Cr(VI) adsorption experiments were conducted at pH 2.5.

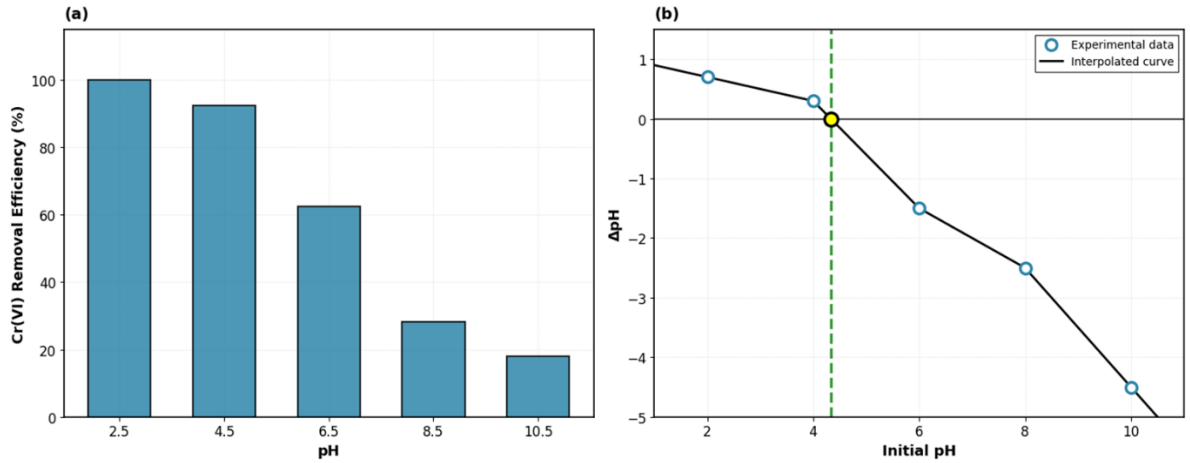

Figure 6: (a) Effect of pH on Cr(VI) removal by mMT (conditions: C_o = 100 mg/L, adsorbent = 50 mg, t = 60 min, T = 25°C); (b) pHPZC determination for mMT

Point of Zero Charge Determination

The pH of point zero charge (pHPZC) for mMT was determined using the solid addition method, and the result is presented in Figure 6b. The pHPZC was found to be approximately 4.4, meaning that the mMT surface carries a net positive charge at pH values below 4.4 and a net negative charge above this value. This finding corroborates the pH-dependent adsorption behavior discussed above, as the maximum Cr(VI) removal occurred at pH 2.5, where the surface is strongly protonated and electrostatically favorable for anion adsorption.

Effect of contact time and adsorption kinetics

The effect of contact time on Cr(VI) adsorption by mMT was investigated at an initial concentration of 100 mg/L, pH 2.5, and adsorbent dose of 50 mg in 100 mL solution. As shown in Figure 7, Cr(VI) removal increased rapidly during the first 30 minutes, with approximately 87% removal achieved within this period. The adsorption gradually slowed and reached equilibrium at about 60 minutes, with a maximum removal efficiency of 99.9%. The initial rapid phase is attributed to the abundant availability of active sites on the mMT surface, while the subsequent slower phase corresponds to the gradual occupation of remaining sites and intraparticle diffusion effects.

For the underlying adsorption mechanism, the experimental data were fitted with pseudo-first-order (PFO; **Eqn. 11**) and pseudo-second-order (PSO; **Eqn. 12**) kinetic models. The pseudo-second-order model provided an excellent fit to the experimental data (R^2 = 0.998), with calculated q_e values closely matching the experimental values (Table 1). This suggests that chemisorption, involving valence forces through electron sharing or exchange between the adsorbent and adsorbate, is the rate-limiting step. The involvement of chemical interactions is consistent with the redox-mediated adsorption mechanism proposed for mMT.

$$\mathrm{In}(q_e - q_t) = \mathrm{In}q_e - k_1 t \qquad 11$$

$$\frac{t}{q_t} = \frac{1}{k_2 q_e^2} + \frac{1}{q_e} t \qquad 12$$

Where, q_e and q_t are the adsorption capacities at equilibrium, and at time t, respectively (mg/g), k_1 and k_2 are respectively the rate constants of PFO and PSO equations (g(mg/min)).

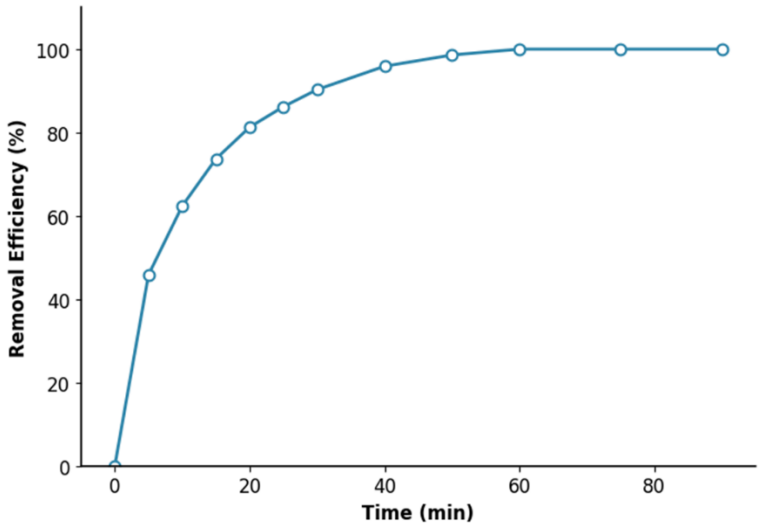

Figure 7: Effect of contact time on Cr(VI) adsorption by Mmt

Table 1: Kinetic Parameters for Cr(VI) Adsorption onto mMT

Kinetic model	Parameter	Value
Experimental	q_e, exp (mg/g)	95.30
Pseudo-first-order	q_e, cal (mg/g)	68.42
	k_1 (min^{-1})	0.072
	R^2	0.912
Pseudo-second-order	q_e, cal (mg/g)	98.04
	k_1 ($g.mg^{-1}\ min^{-1}$)	0.0018
	R^2	0.998

Effect of Cr(VI) concentration and adsorption isotherms

The effect of initial Cr(VI) concentration on adsorption capacity was investigated over the range of 10-100 mg/L at pH 2.5 and at room temperature. As shown in Figure 8, the adsorption capacity (q_e) increased progressively with increasing initial concentration, from 18.6 mg/g at 10 mg/L to 176.4 mg/g at 100 mg/L. This trend is attributed to the higher driving force provided by the increased concentration gradient, which overcomes mass transfer resistance between the aqueous and solid phases. The equilibrium data were analyzed using Langmuir and Freundlich isotherm models. The Langmuir model assumes monolayer adsorption onto a homogeneous surface with finite identical sites, while the Freundlich model describes multilayer adsorption on heterogeneous surfaces. The Langmuir model provided a better fit (R^2 ~0.996) compared to the Freundlich model (R^2 ~0.931), suggesting that removal of Cr(VI) occurs via monolayer coverage on a homogeneous surface, Table 2. The q_{max} calculated from the Langmuir model was 179.31 mg/g, which compares favorably with other biosorbents reported in recent literature (Table 3). The relatively high adsorption capacity of mMT compared to other biosorbents can be attributed to the synergistic effects of: (i) the abundant oxygen-containing functional groups introduced by $KMnO_4$ modification, (ii) the redox-active MnOx species that may facilitate redox transformation and/or reduction of Cr(VI), and (iii) preserved structural integrity that provides accessible binding sites. Nevertheless, future work will include XPS and chromium speciation analysis to quantitatively confirm the extent of Cr(VI) reduction during adsorption.

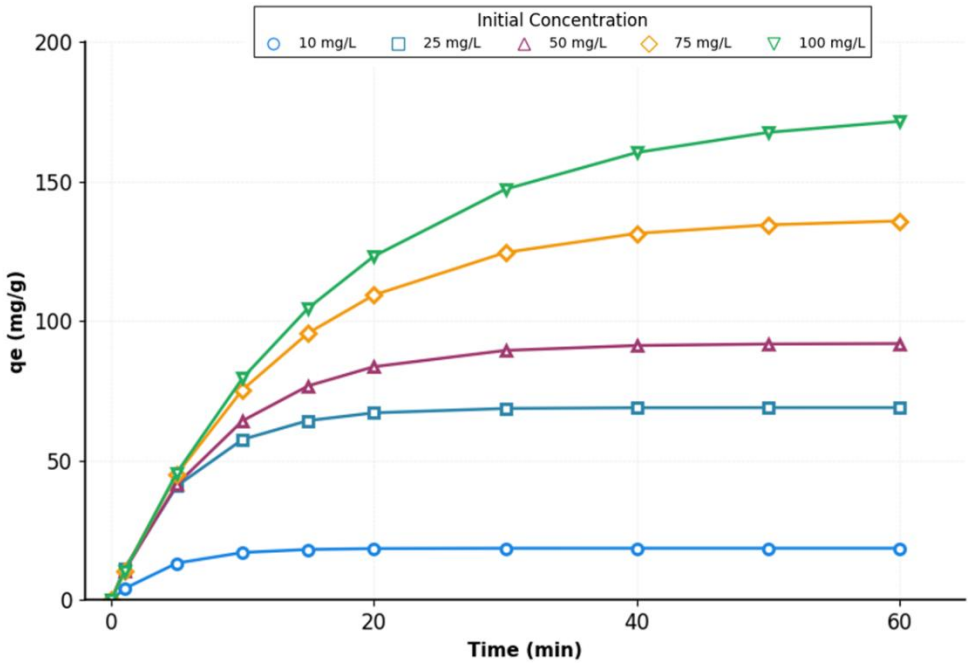

Figure 8: The time-concentration profiles of Cr(VI) adsorption process at different initial concentrations.

Table 2: Isotherm Parameters for Cr(VI) Adsorption onto mMT

Parameter	Langmuir	Freundlich
q_{max} (mg g^{-1})	179.31	-
K_L (L mg^{-1})	0.184	-
K_F (mg/g)(L/mg)$^{1/n}$	-	38.47
n	-	2.36
R^2	0.996	0.931

Table 3: Comparison of adsorption capacities of various biosorbents for Cr(VI)

Biomass	Oxidant	pH	Time (min)	Percentage removal (%)	Ref.
Walnut	NaOH	2.0	60	73.40	33
	Citric acid	2.0	60	68.98	
	-	2.	60	63.78	
Teff straw	H_3PO_4	2	240	92.5	34
	KOH	2	240	95.2	
chinar leaves	$KMnO_4$ and $AlCl_3{\cdot}6H_2O$	3	300	83.86	28
Rice husk	1-[3-(trimethoxysilyl) propyl] urea	2	120	97	35
Poultry litter	H_2SO_4	2	90	-	36
Tea waste	Polyvinyl alcohol	2	300	96	37
Rice husk	boiling water	2		71.0	38
	Formadehyde	2		76.5	
Olive pomace	H_2PO_4	2	240	96	39
Money tree shell	$KMnO_4$	2.5	60	99	This study

Effect of Ionic Strength and Interfering Ions

Real wastewater typically contains various coexisting ions that may compete with Cr(VI) for active adsorption sites. The effect of ionic strength on Cr(VI) adsorption was investigated by adding different concentrations of NaCl, ranging from 0 to 1.0 M (Figure 9a). Increasing NaCl concentration from 0 to 1.0 M resulted in a gradual decrease in removal efficiency from 95.3% to 78.6%. This reduction is attributed to the screening effect of electrolyte ions [40], which weakens the electrostatic interaction between the positively charged mMT surface and Cr(VI) anions.

The influence of coexisting anions, including SO^{2-}_4, NO^-_3, PO^{3-}_4, and CO^{2-}_3, and cations (Ca^{2+}, Na^+, Mg^{2+}) on Cr(VI) removal was examined at a concentration of 0.1 M for each ion (Figure 9b). It is noteworthy to mention that PO^{3-}_4 exhibited the strongest interference among the anions tested, reducing adsorption efficiency of Cr(VI) from 95.3% to 63.2%, followed by CO^{2-}_3, SO^{2-}_4, and NO^-_3 at adsorption efficiencies of 71.4%, 82.1%, and 89.3%, respectively. The significant interference by PO^{3-}_4 and CO^{2-}_3 is attributed to their high charge density and specific adsorption onto the mMT surface, which competes directly with Cr(VI) for binding sites [41]. Additionally, these

anions may form complexes with surface Mn species, potentially blocking redox-active sites. The cations showed relatively minor interference, with Mg^{2+} and Ca^{2+} marginally reducing performance efficiency to 91.2% and 92.4%, respectively. The slight reduction may result from competition for negatively charged surface sites or the formation of cation-chromate complexes in solution that have different adsorption affinities.

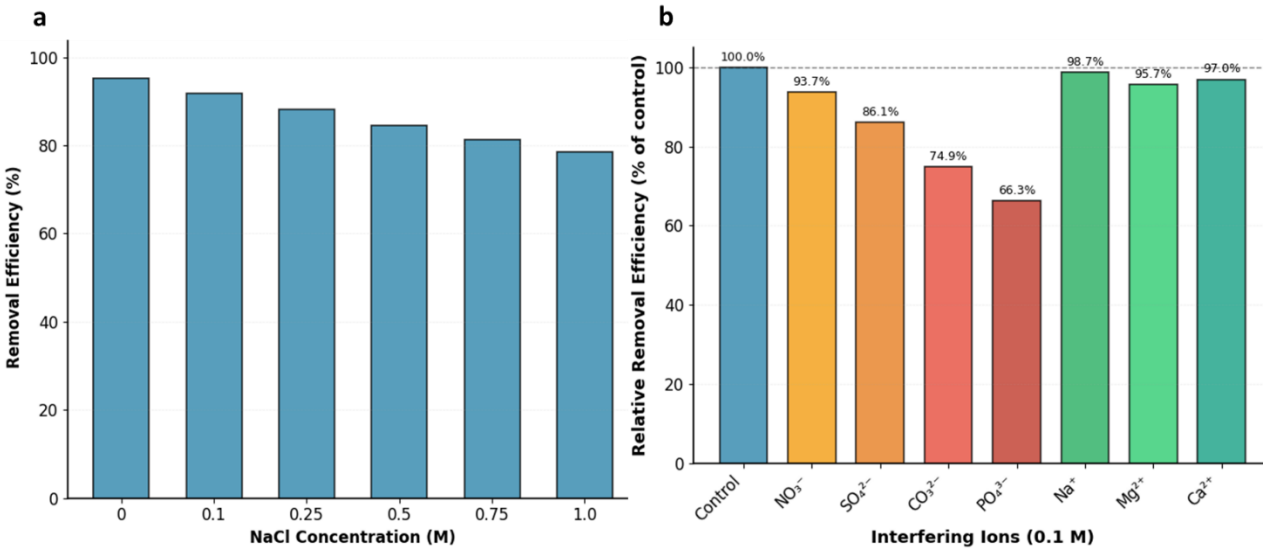

Figure 9: (a) Effect of ionic strength on Cr(VI) adsorption by mMT; (b) Effect of coexisting ions on Cr(VI) removal efficiency

Adsorption thermodynamics

The temperature effect on the removal of Cr(VI) by mMT was investigated at 25ºC, 35ºC, and 45ºC. Thermodynamic parameters such as Gibbs free energy change (ΔGº), enthalpy change (ΔHº), and entropy change (ΔSº) were calculated using the following **Eqns. 13- 15**:

$K_d = q_e/C_e$ 13

$\Delta G^o = -RT \ln K_d$ 14

$\ln K_d = \Delta S^o/R - \Delta H^o/RT$ 15

Table 4 shows negative ΔG° values for all temperatures, confirming that the adsorption process of Cr(VI) is spontaneous. The decrease in magnitude of ΔGº with increasing temperatures from 25ºC to 45ºC indicates that the sorption process is more favourable at higher temperatures.

In Table 5, the positive value of ΔHº (that is + 28.64 kJ/mol) suggests that the sorption process is endothermic, and the absorption of heat enhances the interaction between $HCrO_4^-/Cr_2O_7^{2-}$ and the mMT surface. The magnitude of ΔH° (28.64 kJ/mol) falls within the range typically associated with chemisorption (20-80 $kJ.mol^{-1}$), suggesting that chemical interactions play a dominant role in the adsorption mechanism. This finding aligns with the kinetic results, which favored the pseudo-second-order model. The positive value of ΔS° value (+112.7 $J.mol^{-1}$ K^{-1}) reflects increased randomness at the solid-solution interface during adsorption, due to the release of hydration water molecules when $HCrO_4^-/Cr_2O_7^{2-}$ ions bind to the mMT surface.

Table 4. Temperature-dependent Gibbs free energy

Temperature (ºC)	ΔGº ($kJ.mol^{-1}$)
25	-4.82
35	-6.07
45	-7.31

Table 5: Temperature-independent thermodynamic constants

Parameter	Value
Enthalpy change (ΔHº) ($kJ.mol^{-1}$)	+28.64
Entropy change (ΔSº) ($J.mol^{-1}$ K^{-1})	+112.7

Desorption and regeneration studies

The reusability of an adsorbent is a critical factor for practical applications. Desorption experiments were conducted using various eluents, including NaOH, EDTA, distilled water, and HCl (Figure 10a). Among these, 0.1 M NaOH showed the highest desorption efficiency (86.4%), indicating that Cr(VI) adsorbed onto mMT can be effectively recovered under alkaline conditions. This pH-dependent desorption is consistent with the

electrostatic nature of the adsorption mechanism, where negatively charged surfaces at high pH repel the Cr(VI) anions.

The regeneration efficiency of mMT over five consecutive adsorption-desorption cycles was evaluated using 0.1 M NaOH as the desorbing agent (Figure 10b). The adsorption capacity decreased gradually from 95.3 $mg.g^{-1}$ in the first cycle to 71.6 $mg.g^{-1}$ in the fifth cycle, representing a retention of approximately 75% of the initial capacity. The gradual decline may be attributed to: (i) incomplete desorption of Cr species, (ii) progressive saturation of redox-active sites, and (iii) minor structural changes in the biomass during repeated use. Despite this decrease, the material maintained reasonably good performance after five cycles, demonstrating its potential for repeated use in wastewater treatment applications.

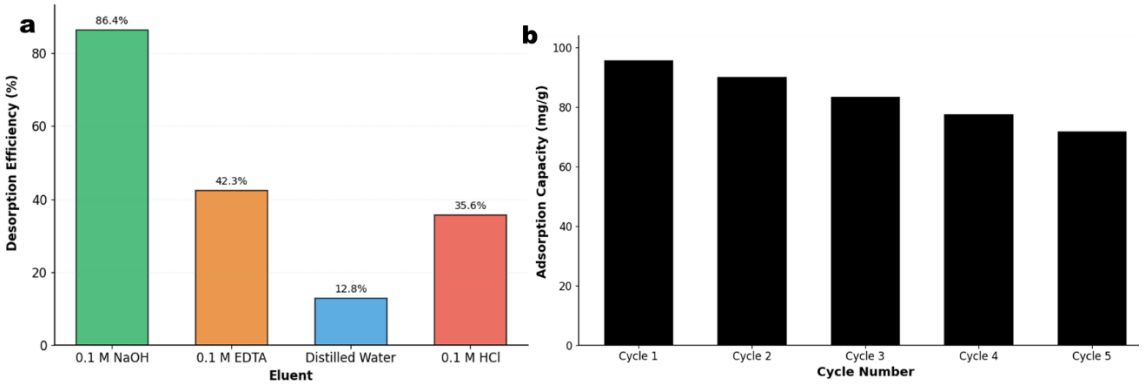

Figure 10: (a) Desorption efficiency of various eluents; (b) Regeneration performance of mMT over five consecutive cycles

IV. Conclusion

This study reports the transformation of empty shells of *Pachira aquatic,* an abundant and typically discarded lignocellulosic biomass, into a high-performance adsorbent for Cr(VI) removal through $KMnO_4$-mediated oxidative modification. The treatment introduced oxygen-containing functional groups and Mn-based redox-active sites, enhancing both the adsorption capacity and the surface-mediated reduction of Cr(VI). Characterization analyses, including FTIR, SEM-EDX, XRD, and TGA confirmed successful surface functionalization and increased accessibility of binding sites. Batch adsorption experiments revealed that the modified biomass (mMT) achieved near-complete Cr(VI) removal at acidic pH, with equilibrium reached within 60 min, and kinetic modeling indicated chemisorption as the rate-limiting step. Adsorption isotherms fitted the Langmuir model, with a maximum capacity of ~179 mg/g, while thermodynamic parameters confirmed that the process is spontaneous and endothermic. The material exhibited good selectivity in the presence of common coexisting ions and retained approximately 75% of its initial capacity over five regeneration cycles. The current work presents a low-cost, sustainable, and efficient biosorbent for Cr(VI) remediation, and provide a practical avenue for valorizing an otherwise underutilized agricultural residue.

Declarations

Funding

This research was funded by the Adekunle Ajasin University Research Grant.

Acknowledgement

The author is grateful to Adekunle Ajasin University, Akungba, Ondo State for the award of research grant to undertake this research work.

References

[1]. Salehi M, Shakiba M, Mazinani S, Abdouss M, Kalaee M. Successful hexavalent chromium removal introducing a novel system composed of aminated polyacrylonitrile nanofiber coated with polysulfide. J Water Process Eng. 2025;69:106683. https://doi.org/10.1016/j.jwpe.2024.106683

[2]. Sharma P, Singh SP, Parakh SK, Tong YW. Health hazards of hexavalent chromium (Cr(VI)) and its microbial reduction. Bioengineered. 2022;13(3):4923–4938. https://doi.org/10.1080/21655979.2022.2037273

[3]. Xie S. Water contamination due to hexavalent chromium and its health impacts: exploring green technology for Cr(VI) remediation. Green Chem Lett Rev. 2024;17(1).

[4]. Mergbi M, Galloni MG, Aboagye D, et al. Valorization of lignocellulosic biomass into sustainable materials for adsorption and photocatalytic applications in water and air remediation. Environ Sci Pollut Res. 2023;30:74544-74574.

[5]. Bhardwaj A, Bansal M, Garima, Wilson K, Gupta S, Dhanawat M. Lignocellulose biosorbents: unlocking the potential for sustainable environmental cleanup. Int J Biol Macromol. 2025;294:139497.

[6]. Yang X, Wan Y, Zheng Y, He F, Yu Z, Huang J, Wang H, Ok YS, Jiang Y, Gao B. Surface functional groups of carbon-based adsorbents and their roles in the removal of heavy metals from aqueous solutions: a critical review. Chem Eng J. 2019;366:608–621. https://doi.org/10.1016/j.cej.2019.02.119

[7]. de Quadros Melo D, Sousa Neto VO, Barros FCF, Raulino GSC, Vidal CB, Nascimento RF. Chemical modifications of lignocellulosic materials and their application for removal of cations and anions from aqueous solutions. J Appl Polym Sci. 2016;133(15).

[8]. Murtazaoğlu Ç, Teğin İ, Saka C. Facile hydrogen peroxide modification of activated carbon particles produced by potassium hydroxide activation for removal of heavy metals from aqueous solutions. Diamond Relat Mater. 2023;136:110049.

[9]. Zhang L, Huang J, Liu X, Luo S, Qu L. Adsorption of Cr(VI) in wastewater by phosphoric acid/nitric acid/oxalic acid modified bagasse. Desalin Water Treat. 2022. https://doi.org/10.5004/dwt.2022.28004

[10]. Sireesha S, Sreedhar I. Phosphorous modified cocopeat biochar as a low cost, efficient and stable adsorbent for the removal of Cu(II) and Ni(II) from aqueous and real systems. Sci Rep. 2025;15:37035.

[11]. Khandgave SS, Sreedhar I. Novel phosphoric acid-modified biochar-chitosan nanocomposite for an efficient and cost-effective multimetal removal from wastewater. ACS Omega. 2025;10(37):42660-42684.

[12]. Wang G, Zhang S, Yao P, et al. Removal of Pb(II) from aqueous solutions by Phytolacca americana L. biomass as a low cost biosorbent. Arab J Chem. 2018;11(1):99-110. https://doi.org/10.1016/j.arabjc.2015.06.011

[13]. Wu H, Lv H, Yu Y, Du Y, Du D. Ammonium persulfate-triggered modified chitosan biochar for co-adsorption of Cr(VI) and tetracycline antibiotics: behavior and mechanisms. Int J Biol Macromol. 2025;311(Pt 2):143432.

[14]. Aguilar KMM, Amano Y, Machida M. Ammonium persulfate oxidized activated carbon fiber as a high capacity adsorbent for aqueous Pb(II). J Environ Chem Eng. 2016;4(4):4644-4652.

[15]. Chen J, Chen Q, Ma Q. Influence of surface functionalization via chemical oxidation on the properties of carbon nanotubes. J Colloid Interface Sci. 2012;370(1):32-38.

[16]. Luo Y. Preparation of MnO_2 nanoparticles by directly mixing potassium permanganate and polyelectrolyte aqueous solutions. Mater Lett. 2007;61(8-9):1893-1895.

[17]. Tong Y, Yan Q, Gao S, Xiong B, Tang X, Liu Z, Li P, Huang M, Wang Z, Le X, Pei W, Dai Z, Xiong Z, Wang Y. Adsorption of Ni^{2+} in aqueous solution by $KMnO_4$ modified biomass: investigation on adsorption kinetics and modification mechanism. Environ Technol. 2022;43(18).

[18]. Zhang Y, Wan Y, Zheng Y, Yang Y, Huang J, Chen H, Quan G, Gao B. Potassium permanganate modification of hydrochar enhances sorption of Pb(II), Cu(II), and Cd(II). Bioresour Technol. 2023;386:129482.

[19]. Deng H, Zhang J, Huang R, Wang W, Meng M, Hu L, Gan W. Adsorption of malachite green and Pb^{2+} by $KMnO_4$-modified biochar: insights and mechanisms. Sustainability. 2022;14(4):2040.

[20]. Lu X, Tian F, Feng Y, Xu X, Wang N, Zhang Q. Sidewall oxidation and complexation of carbon nanotubes by base-catalyzed cycloaddition of transition metal oxide: a theoretical prediction. Nano Lett. 2002;2(12):1325-1327.

[21]. Hernadi K, Siska A, Thien-Nga L, Forró L, Kiricsi I. Reactivity of different kinds of carbon during oxidative purification of catalytically prepared carbon nanotubes. Solid State Ionics. 2001;141-142:203-209.

[22]. Feng YC, Zhou GM, Wang GP, Qu MZ, Yu ZL. Removal of some impurities from carbon nanotubes. Chem Phys Lett. 2003;375:645-648.

[23]. Bankole OM, Oyeneyin OE, Olaseni SE, Akeremale OK, Adanigbo P. Kinetics and thermodynamic studies for Rhodamine B dye removal onto graphene oxide nanosheets in simulated wastewater. Am J Appl Chem. 2019;7(1):10-24. https://doi.org/10.11648/j.ajac.20190701.12.

[24]. Zhao F, Shan R, Gu J, Zhang Y, Yuan H, Chen Y. Magnetically recyclable loofah biochar by $KMnO_4$ modification for adsorption of Cu(II) from aqueous solutions. ACS Omega. 2022;7:8844-8853.

[25]. Dose WM, Donne SW. Manganese dioxide structural effects on its thermal decomposition. Mater Sci Eng B. 2011;176(15):1169-1177.

[26]. Yaman E, Özbay N. Effect of different pre-treatment techniques on thermogravimetric characteristics and kinetics of lignocellulosic biomass pyrolysis. J Energy Inst. 2023;111:101419.

[27]. Majumder R, Sheikh L, Naskar A, Vineeta, Mukherjee M, Tripathy S. Depletion of Cr(VI) from aqueous solution by heat dried biomass of a newly isolated fungus Arthrinium malaysianum: a mechanistic approach. Sci Rep. 2017;7:11254. https://doi.org/10.1038/s41598-017-10160-0.

[28]. Yang J, Song Y, Yue Y, Liu W, Che Q, Chen H, Ma H. Chemically dual-modified biochar for the effective removal of Cr(VI) in solution. Polymers. 2022;14(1):39. https://doi.org/10.3390/polym14010039

[29]. Wang H, Wang W, Zhou S, Gao X. Adsorption mechanism of Cr(VI) on woody-activated carbons. Heliyon. 2023;9(2):e13267. https://doi.org/10.1016/j.heliyon.2023.e13267

[30]. Zhang X, Hua J, Zhu Y, Ding X, Zhang Q, Zhang T, Yang D, Qiu F. Birnessite-type MnO_2 modified sustainable biomass fiber toward adsorption removal of heavy metal ions from actual river aquatic environment. Langmuir. 2024;40(16).

[31]. Sena MM, Scarminio IS, Collins KE, Collins CH. Speciation of aqueous chromium(VI) solutions with the aid of Q-mode factor analysis followed by oblique projection. Talanta. 2000;53(2):453-461.

[32]. Cuong DV, Wu P-C, Chen L-I, Hou C-H. Active MnO_2/biochar composite for efficient As(III) removal: insight into the mechanisms of redox transformation and adsorption. Water Res. 2021;188:116495.

[33]. Garg R, Garg R, Sillanpää M, Alimuddin, Khan MA, Mubarak NM, Tan YH. Rapid adsorptive removal of chromium from wastewater using walnut-derived biosorbents. Sci Rep. 2023;13:6859.

[34]. Ayele AL, Tizazu BZ, Wassie AB. Chemical modification of *Teff straw* biomass for adsorptive removal of Cr(VI) from aqueous solution: characterization, optimization, kinetics, and thermodynamic aspects. Adsorpt Sci Technol. 2022;2022:5820207.

[35]. Ali A, Alharthi S, Al-Shaalan NH, Naz A, Fan HJS. Efficient removal of hexavalent chromium (Cr(VI)) from wastewater using amide-modified biochar. Molecules. 2023;28(13):5146. https://doi.org/10.3390/molecules28135146

[36]. Ghanim B, Leahy JJ, O'Dwyer TF, Kwapinski W, Pembroke JT, Murnane JG. Removal of hexavalent chromium (Cr(VI)) from aqueous solution using acid-modified poultry litter-derived hydrochar: adsorption, regeneration and reuse. J Chem Technol Biotechnol. 2022;97(1):55-66.

[37]. Kabir MM, Sultana F, Rahman MM, Uddin MK. Chromium (VI) removal efficacy from aqueous solution by modified tea wastes-polyvinyl alcohol (TW-PVA) composite adsorbent. Desalin Water Treat. 2020;174:311-323. https://doi.org/10.5004/dwt.2020.24854

[38]. Bansal M, Garg U, Singh D, Garg VK. Removal of Cr(VI) from aqueous solutions using pre-consumer processing agricultural waste: a case study of rice husk. J Hazard Mater. 2009;162(1):312–320. https://doi.org/10.1016/j.jhazmat.2008.05.037

[39]. Alouiz I, Benhadj M, Harboul K, Boukhris M, Elmontassir D, Sennoune M, Amarouch MY, Mazouzi D. Activated carbon from olive pomace for hexavalent chromium removal: synthesis, characterization, and adsorption mechanism analysis. Sci Rep. 2025;15:18576.

[40]. Hu D, Han R, Fei H, Zheng K, Zhang B. ZVI and ball milling co-modified biochar for chromium (Cr(VI)) removal from groundwater: performance optimization and mechanisms. Colloids Surf A Physicochem Eng Asp. 2025;714:136574.

[41]. Fan C, Guo C, Chen W, Tao L, Yao Q, Lu G, Shen Y, Dang Z. Chromate and phosphate adsorption on schwertmannite: competition, mobilization and mechanisms. Colloids Surf A Physicochem Eng Asp. 2023;658:130691.